


## Exceptional Points of Degeneracy Induced by Linear Time-Periodic Variation

Hamidreza Kazemi, Mohamed Y. Nada, Tarek Mealy, Ahmed F. Abdelshafy, and Filippo Capolino\*  
*Department of Electrical Engineering and Computer Science, University of California, Irvine, California 92697, USA*

 (Received 6 April 2018; revised manuscript received 16 September 2018; published 4 January 2019)

We present a general theory of exceptional points of degeneracy (EPD) in periodically time-variant systems. We show that even a single resonator with a time-periodic component is able to develop EPDs, contrary to parity-time- ( $PT$ ) symmetric systems that require two coupled resonators. An EPD is a special point in a system parameter space at which two or more eigenmodes coalesce in both their eigenvalues and eigenvectors into a single degenerate eigenmode. We demonstrate the conditions for EPDs to exist when they are directly induced by time-periodic variation of a system without loss and gain elements. We also show that a single resonator system with zero time-average loss-gain exhibits EPDs with purely real resonance frequencies, yet the resonator energy grows algebraically in time since energy is injected into the system from the time-variation mechanism. Although the introduced concept and formalism are general for any time-periodic system, here, we focus on the occurrence of EPDs in a single  $LC$  resonator with time-periodic modulation. These findings have significant importance in various electromagnetic and photonic systems and pave the way for many applications, such as sensors, amplifiers, and modulators. We show a potential application of this time-varying EPD as a highly sensitive sensor.

DOI: [10.1103/PhysRevApplied.11.014007](https://doi.org/10.1103/PhysRevApplied.11.014007)

### I. INTRODUCTION

Frequency splitting phenomena at exceptional points of degeneracy (EPDs) are adopted to serve in sensing applications [1,2]. Frequency splitting occurs at degenerate resonance frequencies where multiple eigenmodes of the system coalesce. Such degenerate resonance frequencies are extremely sensitive to small changes in the system, which lead to a detectable shift in the system variables. This concept is used in modern sensing devices such as optical microcavities [2–4], bending curvature sensors [5], and optical gyroscopes [6,7].

The splitting point of degenerate resonance frequencies varying a system parameter is referred to as an EPD and it emerges in a system when two or more eigenmodes coalesce in both their eigenvalues and eigenvectors into a single degenerate eigenmode. The concept of EPDs has received a surge of interest in recent years [8–16]. EPDs have been found in non-Hermitian parity-time- ( $PT$ ) symmetric coupled systems, i.e., systems with balanced gain and loss [9,11,14,17,18]. EPDs based on the concept of  $PT$  symmetry have been investigated in coupled waveguides whose eigenmodes' evolution is described in space [1,8,19], and also in coupled resonators where the eigenmodes' evolution is described in time [10,12,15,20]. EPDs may also exist in lossless-gainless periodic waveguides, which support multiple polarization eigenmodes that are

periodically mixed and usually occur at the transmission band edge [13,21–30]. In essence, EPDs are obtained when the system matrix is similar to a matrix that contains a Jordan block [23,31,32]. At the EPD, the system eigenstate is represented in terms of generalized eigenvectors rather than the regular eigenvectors [22,23], which, in turn, leads to algebraic growth in the system eigenstates [23,32]. There are different unique properties associated with the emergence of EPDs, which lead to various potential applications, such as enhancing the gain of active systems [16,33–37], directivity in antennas [38], enhanced sensors [1,2,39], etc.

We demonstrate the occurrence of EPDs directly induced by temporal-periodic variation of a system. The newly introduced concept for systems that are periodically time varying is analogous to EPDs found in spatially periodic waveguides [13,16,21–24,28,30].

In Fig. 1, we show two examples of temporally periodic systems that exhibit EPDs. Note that time variation was already considered in  $PT$ -symmetric systems with EPDs [40–44]. The time variation was used to enhance some features in systems that had already developed EPDs due to  $PT$  symmetry. In contrast, in this paper, we show that EPDs are directly induced in a single resonator by periodic time variation of the system itself, without the need for elements that exhibit time-invariant gain. As an example, we demonstrate the concept using the simplest possible resonator, i.e., an  $LC$  resonator, though the formalism is general and applicable to any time-periodic photonic or

\*f.capolino@uci.edu

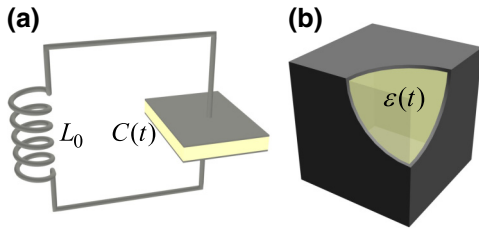


FIG. 1. Two examples of systems with time-periodic variation: (a)  $LC$  resonator with a time-varying capacitor  $C(t)$ . (b) Metallic resonator filled with a dielectric that has a time-varying permittivity  $\epsilon(t)$ . These single resonators are able to exhibit EPDs when a precise modulation frequency is applied.

radio frequency system. Remarkably, we demonstrate that the occurrence of EPDs is solely due to time-periodic variations in a linear time-periodic (LTP) system. Hence, the presence of time-invariant gain or loss (namely a transistor, a pumped active medium, or material losses) is not necessary to generate an EPD. When an EPD is directly induced by time modulation, as proposed in this paper, the system receives energy in a subtle way through the time-variation process. Therefore, in an LTP system, the EPD is simply obtained by tuning the period of the time modulation, which is a standard practice in many engineering applications, in contrast to  $PT$ -symmetric systems where the requirements on gain and loss elements may be difficult to achieve in practice. Moreover, gain elements always include parasitic reactances that have to be included in any  $PT$ -symmetric double-resonator realistic design.

In Sec. II, we provide the general theory and formulation for EPDs to exist in linear time-periodic systems. We also show that even a single passive resonator (without gain or loss elements such as transistors or negative resistors) exhibit EPDs once time-periodic modulation is introduced. Then we further investigate two other linear time-periodic systems that include negative resistance and we derive the necessary and sufficient conditions for second-order EPDs to occur. Finally, we show how a simple resonator with time modulation can perform as an extremely sensitive sensor.

## II. FORMULATION FOR EPD INDUCED BY TIME-PERIODIC VARIATION

Time-periodic variation is introduced in a system through any time-varying system parameter. Generally, an LTP system may be comprised of multiple components, therefore, we will assume that the state vector  $\Psi(t)$  describing this system is  $N$ -dimensional, i.e.,

$$\Psi(t) = [\Psi_1(t) \cdots \Psi_N(t)]^T, \quad (1)$$

where  $T$  denotes the transpose operator. The temporal evolution of the state vector obeys the multidimensional

first-order differential equation

$$\frac{d}{dt}\Psi(t) = \underline{\mathbf{M}}(t)\Psi(t), \quad (2)$$

where  $\underline{\mathbf{M}}(t)$  is the  $N \times N$  time-variant system matrix. For LTP systems with period  $T_m$ , the state vector evolution from the time instant  $t$  to  $t + T_m$  is given by

$$\Psi(t + T_m) = \underline{\Phi}(t + T_m, t)\Psi(t), \quad (3)$$

where  $\underline{\Phi}(t + T_m, t)$  is the state transition matrix [45]. In the following, for simplicity and without loss of generality, we assume the matrix  $\underline{\mathbf{M}}(t)$  is represented by a piecewise constant periodic function, hence, we relate the transition matrix to the system matrices as

$$\underline{\Phi} = \prod_{j=1}^J e^{\underline{\mathbf{M}}_j T_j}, \quad (4)$$

where  $\underline{\mathbf{M}}_j$  is the system matrix in the  $j$ th interval  $T_j$ , and the system modulation frequency is  $f_m = 1/T_m$  where  $T_m = \sum_{j=1}^J T_j$ . Solutions of an LTP system in general satisfy

$$\Psi(t + T_m) = e^{-i\omega T_m} \Psi(t), \quad (5)$$

which means that  $\Psi(t)$  can be represented in terms of the Floquet harmonics. Using the transition matrix to represent the time evolution of the state vector, we formulate the eigenvalue problem as

$$\underline{\Phi}\Psi(t) = \lambda\Psi(t). \quad (6)$$

The eigenvalues  $\lambda_n = \exp(-i\omega_n T_m)$ ,  $n = 1, \dots, N$ , with  $\omega_n$  being the system eigenfrequencies, are obtained by solving the characteristic polynomial

$$\det(\underline{\Phi} - \lambda\underline{\mathbf{I}}) = 0. \quad (7)$$

When the transition matrix is diagonalizable, we can write  $\underline{\Phi} = \underline{\mathbf{U}}\underline{\Lambda}\underline{\mathbf{U}}^{-1}$ , where  $\underline{\mathbf{U}}$  is a nonsingular similarity transformation matrix whose columns are the eigenvectors of  $\underline{\Phi}$  that are all independent. This analysis is valid unless an EPD emerges at which the transition matrix  $\underline{\Phi}$  is nondiagonalizable and it is similar to a matrix  $\underline{\Lambda}_J$  that contains at least a nontrivial Jordan block with  $P$  degenerate eigenvalues [32]. Therefore, at the EPD, the algebraic multiplicity  $P$  of an eigenvalue  $\lambda_e$  (and its correspondent eigenfrequency  $\omega_e$ ) of (6) is higher than its geometrical multiplicity (the number of independent eigenvectors associated with that eigenvalue) because two or more eigenvectors coalesce. The similarity transformation at the EPD is written as  $\underline{\Phi} = \underline{\mathbf{V}}\underline{\Lambda}_J\underline{\mathbf{V}}^{-1}$  where the columns of  $\underline{\mathbf{V}}$  are composed of

regular eigenvectors and generalized eigenvectors that are found through

$$(\underline{\Phi} - \lambda_e \mathbf{I})^p \Psi_p(t) = \mathbf{0}, \quad p = 1, 2, \dots, P. \quad (8)$$

Here,  $\Psi_p$  with  $p > 1$  are the generalized eigenvectors and  $P$  is the order of degeneracy (see Chap. 7 in [31]).

### III. TIME-VARIYING INDUCED SECOND-ORDER EPD

For the sake of simplicity, the following analysis and examples focus on second-order EPDs that emerge in LTP systems, hence the transition matrix  $\underline{\Phi}$  has dimensions  $2 \times 2$ . For a system described by a real  $2 \times 2$  transition matrix, the characteristic polynomial  $\det(\underline{\Phi} - \lambda \mathbf{I}) = 0$  has real coefficients so that the eigenvalues  $\lambda_1$  and  $\lambda_2$  are either both real or are a complex conjugate pair. Since the determinant of the matrix can be expressed as

$$\det(\underline{\Phi}) = \lambda_1 \lambda_2 = \prod_{j=1}^2 e^{\text{tr}(\underline{M}_j T_j)}, \quad (9)$$

where  $\text{tr}$  denotes the trace of the matrix, then the determinant can be either

$$\det(\underline{\Phi}) = e^{2\text{Im}\{\omega_1\}T_m}, \quad (10)$$

when  $\lambda_2 = \lambda_1^*$ , where the symbol  $*$  denotes the complex conjugate operation, or

$$\det(\underline{\Phi}) = e^{is\pi} e^{(\text{Im}\{\omega_1\} + \text{Im}\{\omega_2\})T_m}, \quad (11)$$

when  $\lambda_1$  and  $\lambda_2$  are both real, where  $\omega_1$  and  $\omega_2$  are the eigenfrequencies of the eigensystem (6) and  $s$  is an integer. At the EPD, the  $2 \times 2$  transition matrix  $\underline{\Phi}$  is similar to a Jordan block with two degenerate eigenvalues that are associated with a regular eigenvector and a generalized eigenvector obtained from (8). On the other hand, the eigenvalues of any  $2 \times 2$  matrix  $\underline{\Phi}$  are [46]

$$\lambda_n = \text{tr}(\underline{\Phi})/2 \pm \sqrt{[\text{tr}(\underline{\Phi})/2]^2 - \det(\underline{\Phi})}, \quad (12)$$

where the upper and lower signs hold for  $n = 1, 2$ . The associated eigenvectors of the system described by a non-diagonal  $\underline{\Phi}$  are

$$\Psi_n = [\phi_{12}, \lambda_n - \phi_{11}]^T, \quad n = 1, 2, \quad (13)$$

where  $\phi_{11}$  and  $\phi_{12}$  are elements of the matrix  $\underline{\Phi}$  [45]. It is clear from the expression of the eigenvectors that degenerate eigenvalues lead to degenerate eigenvectors (i.e., identical eigenvectors) unless the matrix  $\underline{\Phi}$  is diagonal. Therefore, to guarantee the emergence of EPDs in a system

described by a nondiagonal transition matrix  $\underline{\Phi}$ , it is sufficient to have degenerate eigenvalues, i.e., it is sufficient to satisfy the condition

$$\text{tr}(\underline{\Phi})/2 = \pm \sqrt{\det(\underline{\Phi})}. \quad (14)$$

The presented formulation is general and describes the occurrence of EPDs in any system described with the set of differential equations in (2). Without loss of generality and to provide a physical description of a  $2 \times 2$  LTP system, we demonstrate all the above concepts by using very simple  $LC$  resonator examples.

#### A. Time-periodic system without gain and loss elements

Consider first the lossless  $LC$  resonator with time-periodic capacitance as depicted in Fig. 2(b); this example demonstrates the existence of EPDs in a simple LTP system made of a lossless and gainless resonator. We define the system state vector as  $\Psi(t) = [q(t) \ i(t)]^T$ , where  $q(t)$  is the instantaneous charge on the capacitor and  $i(t)$  is

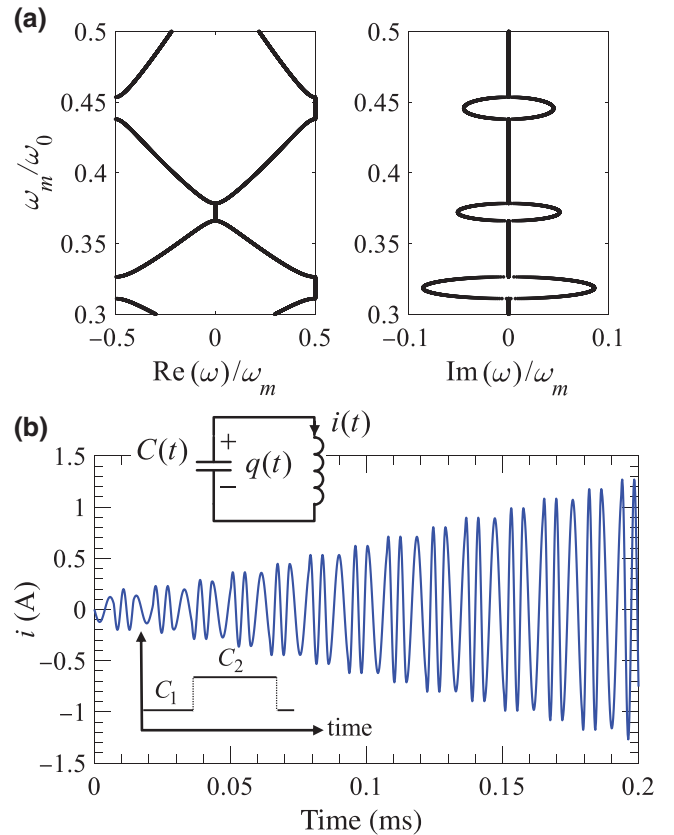


FIG. 2. (a) Real and imaginary parts of dispersion diagram of the eigenfrequencies (complex resonance frequencies  $\omega$ ) vs normalized modulation angular frequency  $\omega_m$ . (b) The linear algebraic growth of the inductor current at an EPD for an  $LC$  resonator with a time-varying capacitor. Therefore, the energy stored in the inductor grows quadratically.

the inductor current as shown in the circuit depicted in Fig. 2(b).

The time-variant capacitor is given by a two-level piecewise constant time-periodic function:  $C_1$  in the interval  $0 \leq t < T_1$  and  $C_2$  in  $T_1 \leq t < T_m$ . The time evolution of the state vector  $\Psi(t)$  is described by (2), where  $\underline{\mathbf{M}}(t) = \underline{\mathbf{M}}_1$  for  $0 \leq t < T_1$  and  $\underline{\mathbf{M}}(t) = \underline{\mathbf{M}}_2$  for  $T_1 \leq t < T_m$ , with

$$\underline{\mathbf{M}}_j = \begin{bmatrix} 0 & -1 \\ 1/(L_0 C_j) & 0 \end{bmatrix}, \quad j = 1, 2. \quad (15)$$

Figure 2(a) illustrates the dispersion of the eigenfrequencies  $\omega$  of  $\underline{\Phi}$ , symmetrically located with respect to the center of the Brillouin zone (BZ), vs the normalized angular modulation frequency ( $\omega_m/\omega_0$ ), where  $\omega_0 = 1/\sqrt{L_0 C_0}$  and  $C_0 = (C_1 + C_2)/2$ . Note that the system is periodic, so that for an eigenfrequency  $\omega$ , there corresponds all the Floquet harmonics  $\omega + s\omega_m$ , where  $s$  is an integer. For the system matrices (15) with real-valued elements, it can be shown that  $\det(\underline{\Phi}) = 1$ , which implies either that  $|\lambda_1| = |\lambda_2| = 1$  (hence,  $\text{Im}\{\omega_1\} = \text{Im}\{\omega_2\} = 0$ ) when  $\lambda_2 = \lambda_1^*$ , or that  $\lambda_2 = 1/\lambda_1$  (hence,  $\text{Im}\{\omega_1\} = -\text{Im}\{\omega_2\}$ ) when both eigenvalues are real. This means that at the EPDs, the degenerate eigenvalue  $\lambda_e = \pm 1$ , therefore,  $\omega_e$  is purely real. This finding agrees with what is shown in the complex dispersion diagram depicted in Fig. 2(a). The parameters of the  $LC$  resonator are set as  $L_0 = 10 \mu\text{H}$ ,  $C_1 = 50 \text{ nF}$ , and  $C_2 = 150 \text{ nF}$ . The two  $\omega$  solutions coalesce for some modulation angular frequencies  $\omega_m$  and become exactly equal at the EPDs. In this particular example, EPDs occur at either the center of the BZ ( $\text{Re}\{\omega\} = 0$ ) or at the edge of the BZ ( $\text{Re}\{\omega/\omega_m\} = \pm 0.5$ ). It is important to point out that for a lossless and gainless system, the imaginary part of the dispersion diagram is symmetric with respect to the center of the BZ and it vanishes at the EPDs, i.e., EPDs occur at real-valued frequencies.

In Fig. 2(b), we show the time-domain simulation of the state vector element  $i(t)$  at one of the EPDs ( $\omega_m = 0.44\omega_0$ ) assuming a capacitor charge initial condition of  $q_c(0^-) = 50 \text{ nC}$ . It is clear from Fig. 2(b) that the capacitor current is growing linearly with time even in the absence of gain element, which resembles one of the most important characteristics associated with the generalized eigenvector of a second-order EPD. Note that even though there is no gain element in the system, the time-periodic  $LC$  resonator is not isolated, and it receives energy from, or provides it to, the time-variation process. The time-variant capacitor in this system can be implemented using a varactor diode where a pump signal changes its capacitance.

The general condition (14) is sufficient for a system described by a nondiagonal  $2 \times 2$  transition matrix to exhibit EPDs. In particular, for the lossless and gainless time-periodic  $LC$  resonator in Fig. 2, this sufficient

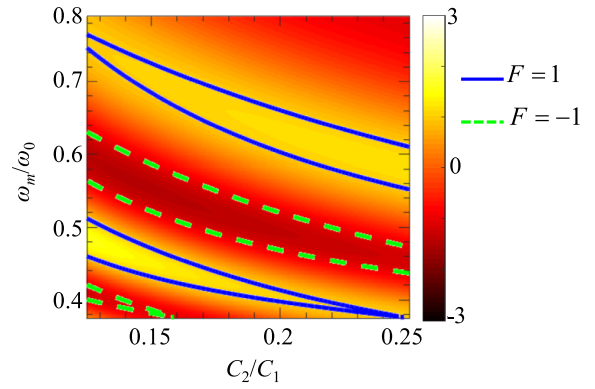


FIG. 3. The function  $F$  of the lossless  $LC$  resonator depicted in Fig. 2(b) vs the capacitance  $C_2$  and the normalized modulation angular frequency  $\omega_m/\omega_0$ . Solid (blue) and dashed (green) contours on the color map represent points which satisfy the EPDs' condition  $F = \pm 1$  in (16).

condition reads

$$F = \cos(\Omega_1 T_1) \cos(\Omega_2 T_2) - \frac{1}{2} \left( \sqrt{\frac{C_1}{C_2}} + \sqrt{\frac{C_2}{C_1}} \right) \sin(\Omega_1 T_1) \sin(\Omega_2 T_2) = \pm 1, \quad (16)$$

where  $\Omega_j = (L_0 C_j)^{-1/2}$  with  $j = 1, 2$  are the resonance frequencies of the  $LC$  resonator in the time intervals  $T_1$  and  $T_2$ , respectively. Figure 3 shows the function  $F$  varying the capacitance  $C_2$  ( $C_1$  is constant) and the normalized angular modulation frequency ( $\omega_m/\omega_0$ ). The solid blue and dashed green contours represent points on the color map where an EPD exists: the blue contours represent points where  $F = 1$ , which are associated with EPDs at the center of the BZ, while the dashed green contours represent points where  $F = -1$ , which are associated with EPDs at the edge of the BZ.

Energy-wise, a time-periodic system (e.g., a time-periodic  $LC$  circuit) is not isolated, and such a system is in a continuous interaction with the source of time variation. Such an interaction can transfer energy into or out of the system, i.e., the system will gain energy from or lose energy to the time-variation source. The procedure of periodically varying the capacitance to add energy to the circuit is referred to as pumping [45,47–49], contrary to adding energy to the system directly from an input source such as a transistor, a time-invariant pump, or an optically active medium, which are referred to in this manuscript as time-invariant gain mechanisms [50,51]. The average energy transfer into or out of an LTP component can be calculated using the time-domain solution of the multidimensional first-order differential equations in (2). It can be easily shown that the state vector of a periodically time-variant system experiencing an EPD grows linearly with



time, and therefore, the average transferred energy to the system will have a quadratic growth.

### B. Time-periodic system with gain and loss elements

As a second example, we show that a system with time-periodic loss and/or gain also exhibits EPDs. To demonstrate the emergence of EPDs in this type of time-periodic system, we use an RLC resonator with time-periodic piecewise constant conductance, as depicted in Fig. 4(b). Analogous to the previous example, we assume a two-level piecewise constant time-periodic conductance:  $G_1$  for  $0 \leq t < T_1$  and  $G_2$  for  $T_1 \leq t < T_m$ . In general,  $G_1$  and  $G_2$  can be positive (representing a loss in the system) or negative (representing a gain). The state vector is defined as  $\Psi(t) = [q(t) \ i(t)]^T$ , with  $q(t)$  as the instantaneous charge on the capacitor and  $i(t)$  as the inductor current. The constant system matrices of the two-time intervals are given by

$$\underline{\mathbf{M}}_j = \begin{bmatrix} -G_j/C_0 & -1 \\ 1/(L_0 C_0) & 0 \end{bmatrix}, \quad j = 1, 2. \quad (17)$$

Such a system develops EPDs in two different scenarios; the first scenario is through using time-periodic conductance with non-zero time average, whereas the second one is through using time-periodic conductance with zero time average, i.e.,

$$G_1 T_1 + G_2 T_2 = 0. \quad (18)$$

In addition, a system with a positive time-average conductance has a dominant loss and a system with a negative time-average conductance has a dominant gain. Moreover, a system with a zero time average has a time-periodic gain and loss balance.

#### 1. Non-zero time-average conductance

Figure 4(a) shows the complex dispersion diagram of a system with a positive time-average conductance (i.e.,  $G_1 T_1 + G_2 T_2 > 0$ ). The parameters of the LC resonator are  $L_0 = 10 \mu\text{H}$ ,  $C_0 = 100 \text{ nF}$ ,  $G_1 = 101 \text{ mS}$ ,  $G_2 = -99 \text{ mS}$ , and  $T_1 = T_2 = T_m/2$ . Figure 4(b) shows the inductor current at an EPD with  $\omega_m = 0.37\omega_0$  and  $q_c(0^-) = 50 \text{ nC}$ .

Note that for all the EPDs in such a system, the imaginary part of the eigenfrequencies is negative, which is a result of the dominant time-average loss in the system and this leads to an exponential decay of the system state vector in addition to the linear algebraic growth (visible at early times) due to the degeneracy.

Similar to the system with a dominant time-periodic loss, a system with a dominant time-periodic gain (i.e.,  $G_1 T_1 + G_2 T_2 < 0$ ) will develop EPDs in its dispersion diagram. However, eigenfrequencies away from the band gaps

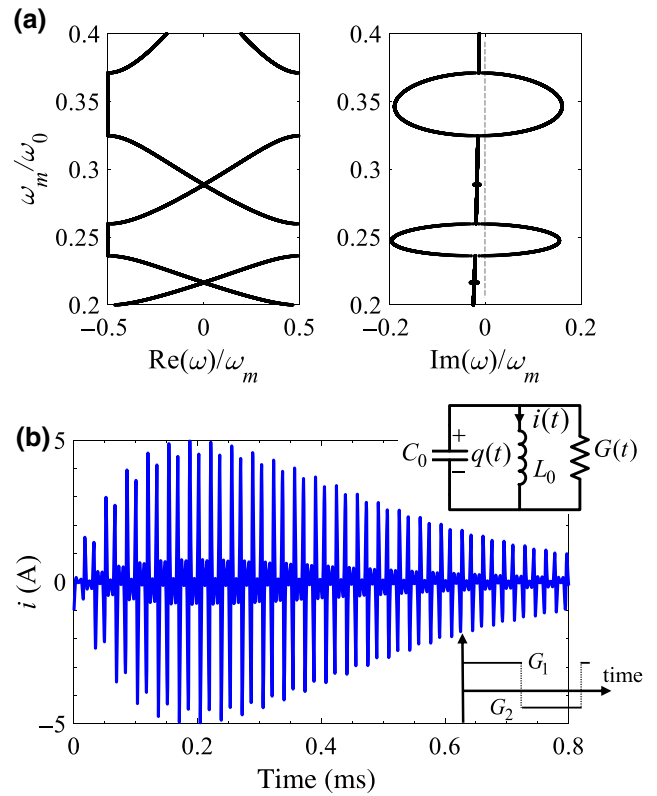


FIG. 4. (a) Dispersion diagram of the eigenfrequencies (complex resonance frequencies  $\omega$ ) of the resonator depicted in (b) vs modulation angular frequency  $\omega_m$ . The vertical dashed line represents the  $\text{Im}\{\omega\} = 0$  to point out that the imaginary part is negative. (b) Time evolution of the inductor current at an EPD for the time-periodic lossy resonator with a positive time-average conductance as shown in the figure.

have a positive imaginary part, which leads to an exponential growth of the state vector with time in addition to the linear growth at the EPD.

#### 2. Zero time-average conductance

The determinant of the transition matrix is

$$\det(\underline{\Phi}) = \prod_{j=1}^2 e^{\text{tr}(\underline{\mathbf{M}}_j T_j)} = e^{-(G_1 T_1 + G_2 T_2)/(2C_0)}, \quad (19)$$

Therefore, when (18) is satisfied,  $\det(\underline{\Phi}) = 1$ , which leads to the same conclusion found for the lossless-gainless LC resonator discussed in relation to Fig. 2. This means that at the EPDs,  $\lambda_e = \pm 1$ , and therefore,  $\omega_e$  is purely real.

Assuming  $T_1 = \alpha T_m$ , then  $T_2 = (1 - \alpha)T_m$ , and assuming  $G_1 > 0$ , then to satisfy the time-average condition (18), the conductance  $G_2 = -\alpha G_1/(1 - \alpha)$ .

The schematic of a time-periodic gain- and loss-balanced LC resonator is depicted in Fig. 5(b) where the time-variant conductance is assumed to satisfy (18). The

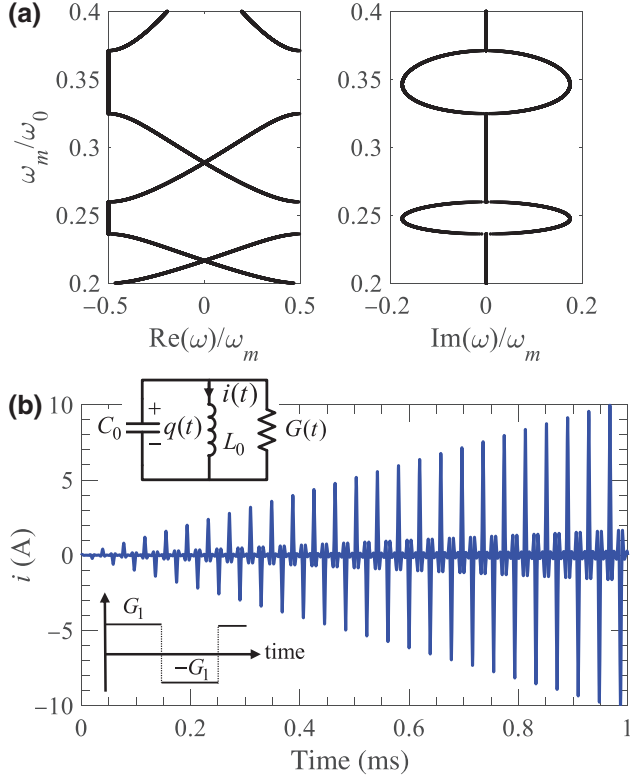


FIG. 5. (a) Dispersion diagram of the eigenfrequencies (complex resonance frequencies  $\omega$ ) of the resonator depicted in (b) vs modulation angular frequency  $\omega_m$ . (b) Algebraic growth of the inductor current at an EPD of the time-periodic gain-loss balanced resonator, where the conductance is temporally periodic with zero time average.

dispersion diagram shown in Fig. 5(a) is based on parameters  $L_0 = 10 \mu\text{H}$ ,  $C_0 = 100 \text{ nF}$ ,  $G_1 = -G_2 = 100 \text{ mS}$ , and  $T_1 = T_2 = T_m/2$ , and modulation frequency  $\omega_m = 0.32\omega_0$  with  $\omega_0 = 1/\sqrt{L_0 C_0}$ . The time-domain evolution of the inductor current  $i(t)$ , assuming an initial capacitance charge  $q_c(0^-) = 50 \text{ nC}$ , is shown in Fig. 5(b). Since the system has a second-order EPD and a time-periodic gain and loss balance, we only observe a dominant linear growth in the current of the resonator at the EPD.

From (14), we find the sufficient condition for EPDs to emerge in a system with time-variant conductance to be

$$F = \cos(\Omega_1 T_1) \cos(\Omega_2 T_2) - \frac{\omega_0^2}{\Omega_1 \Omega_2} \left[ 1 - \frac{G_1 G_2}{4G_0^2} \right] \sin(\Omega_1 T_1) \sin(\Omega_2 T_2) = \pm 1, \quad (20)$$

where  $G_0 = \sqrt{C_0/L_0}$  and  $\Omega_j = \omega_0 \sqrt{1 - G_j^2/(4G_0^2)}$ ,  $j = 1, 2$ , are the real parts of the complex resonance

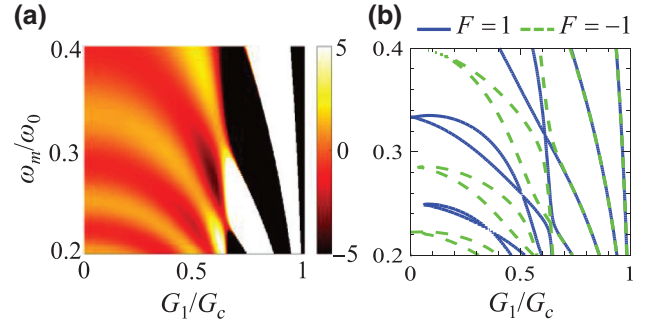


FIG. 6. (a) The function  $F$  in terms of the conductance  $G_1$  and the normalized modulation angular frequency  $\omega_m/\omega_0$  for  $\alpha = 0.6$ . (b) Contours of points which satisfy the EPD condition in (20).

frequencies for the resonator in the time intervals  $T_1$  and  $T_2$ , respectively. In Fig. 6(a), we show the function  $F$  vs conductance  $G_1$  and the normalized angular modulation frequency  $\omega_m/\omega_0$ , where we assume a zero time-average conductance with  $\alpha = 0.6$ . There exists a critical value of the conductance  $G_1$  that is denoted by  $G_c = 2G_0 \max\{1, (1 - \alpha)/\alpha\}$ , beyond which both  $\Omega_1$  and  $\Omega_2$  become purely imaginary and the system cannot exhibit EPDs. In Fig. 6(b), the solid blue contours ( $F = 1$ ) and the dashed green contours ( $F = -1$ ) represent points on the color map where an EPD exists.

#### IV. SENSITIVITY TO SYSTEM PERTURBATION

As discussed in the introduction, the eigenvalues at the EPDs are extremely sensitive to the perturbations of the system parameters. In general, introducing a perturbation  $\varepsilon$  to any of the system parameters leads to a perturbed transition matrix  $\Phi(\varepsilon)$  and perturbed eigenvalues  $\lambda_p(\varepsilon)$ , with  $p = 1, 2, \dots, P$  where  $P$  is the order of the EPD. We represent  $\lambda_p(\varepsilon)$  near the EPD eigenvalue  $\lambda_e$  by a single convergent Puiseux series containing only powers of  $\varepsilon^{1/P}$ , where the Puiseux series coefficients are calculated using the explicit recursive formulas given in [52]. For a second-order EPD ( $P = 2$ ), we use a first-order approximation of  $\lambda_p(\varepsilon)$  as

$$\lambda_p(\varepsilon) \approx \lambda_e + (-1)^p \alpha_1 \sqrt{\varepsilon}, \quad (21)$$

where

$$\alpha_1 = \sqrt{-\partial f(\varepsilon, \lambda)/\partial \varepsilon} \Big|_{\varepsilon=0, \lambda=\lambda_e}, \quad (22)$$

and  $f(\varepsilon, \lambda) = \det[\Phi(\varepsilon) - \lambda \mathbf{I}]$ . As an illustrative example, consider an  $LC$  resonator with time-variant capacitance as described in Fig. 2, but with a lossy inductor with a quality factor of 100, and assume  $C_2$  is now perturbed from its nominal value as  $(1 + \varepsilon) C_2$ . When  $C_2$  is not perturbed, the system exhibits an EPD with an eigenvalue

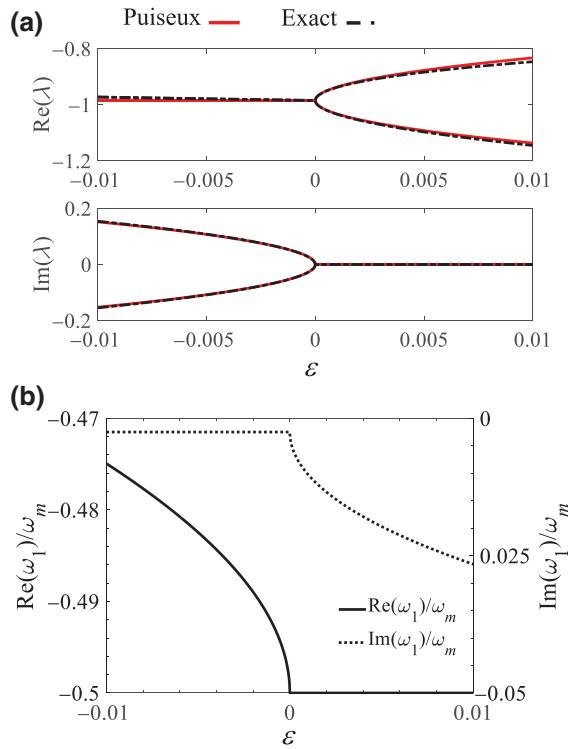


FIG. 7. (a) Variation of the eigenvalues away from the EPD of a lossy LC resonator as in Fig. 2(b), but with a lossy inductor, when the capacitor  $C_2$  is perturbed. (b) The complex resonance frequency  $\omega_1$  exhibits large variations even for very small perturbations  $\varepsilon$ .

$\lambda_e = -0.98$  for a modulation frequency  $\omega_m = 0.44\omega_0$ . In Fig. 7(a), we show the two perturbed eigenvalues  $\lambda$  vs the perturbation  $\varepsilon$  calculated from the exact eigenvalue problem (6) and by using the Puiseux series approximation. The most important thing to notice from Fig. 7 is that an extremely small perturbation in capacitor  $C_2$  will lead to a much larger change in the eigenvalues of the system. This property is actually one of the most exceptional physical properties associated with EPDs and it can be exploited in designing extremely sensitive sensors [8,15]. The large perturbation of the eigenvalues, in turn, implies a sharp change in the complex resonance frequency of the LTP LC resonator as shown in Fig. 7(b). For a positive but very small  $\varepsilon$ -perturbation, the imaginary part of the complex resonance frequency shows a sharp change, while its real part remains constant. Furthermore, a very small negative  $\varepsilon$ -perturbation causes a rapid change of the real part of the resonance frequency. For example, a  $+0.1\%$  perturbation in the dielectric permittivity of the capacitor  $C_2$  (i.e.,  $\varepsilon = 0.001$ ) will change the imaginary part of the resonance frequency by  $0.34\omega_0$ , which implies 76% change in the quality factor of the resonator. Hence, this highly sensitive system can be employed to measure the dielectric permittivity (that can be changed by an environmental

parameter, such as acidity or humidity, or a gas presence) with very high accuracy.

## V. CONCLUSION

Time-periodic systems support EPDs of different orders directly induced by the time modulation of a parameter of the system. Therefore, the existence of an EPD does not require the presence of time-invariant gain or loss elements in the system as implied in all the  $PT$ -symmetry examples shown in the literature. Forced time variation of a system element is another way to inject energy into the system, and the EPD is obtained by properly tuning the modulation frequency. The proposed way to obtain EPDs, directly induced by periodic-time variation, enables even single resonators to exhibit EPDs, in contrary to the minimum of two resonators as implied by  $PT$  symmetry. Indeed, in this paper, the time variation is not used to enhance the properties of EPDs, but rather as a way to generate EPDs.

Second-order EPDs are demonstrated analytically and supported with examples. We have shown the analytic sufficient conditions for such EPDs to exist. Also, we have demonstrated that in the absence of any time-invariant gain- and loss-circuit elements, the resonance frequency of an EPD is purely real. Furthermore, this property also holds when gain and loss elements are explicitly introduced in the system, assuming that the time average of the gain and loss is zero. At the second-order EPDs, the energy inside a time-periodic resonator grows quadratically with time even when the resonance frequency is purely real, with the injected energy coming from the time-modulation process. Moreover, we have illustrated how such temporally induced EPDs lead to systems where the eigenvalue (i.e., the complex eigenfrequency) is exceptionally sensitive to a perturbation of the system. This may have potential applications in conceiving highly-sensitive devices.

In summary, the proposed way to obtain EPDs via time modulation may present practical advantages compared to  $PT$ -symmetric systems, since a single resonator is sufficient to obtain an EPD as shown in this paper by just introducing time modulation to one of its elements. Moreover, in many engineering applications, it is easier to tune the modulation frequency than to realize devices with a precise gain amount as required in  $PT$ -symmetric systems because gain devices possess parasitic reactances that have to be included in any design.

## ACKNOWLEDGMENT

This material is based upon work supported by the Air Force Office of Scientific Research under Grant No. FA9550-15-1-0280 and by the National Science Foundation under Grant No. ECCS-1711975. The authors acknowledge useful discussions with Professor Franco

Maddaleno, Polytechnic of Turin, and with Professor Alexander Figotin, University of California, Irvine.

### APPENDIX: ANALYTICAL TIME-DOMAIN SOLUTION OF THE EVOLUTION EQUATIONS

An analytical time-domain solution of the evolution equation in (2) with a two-level piecewise coefficient can be obtained using the method explained in Ref. [45], where the state vector  $\Psi(t)$  at any time instant  $t = mT_m + \chi$ , with  $\chi < T_m$  is

$$\Psi(t) = \underline{\Phi}(\chi, 0)\underline{\Phi}^m(T_m, 0)\Psi(0), \quad (\text{A1})$$

where  $\Psi(0)$  is the initial condition of the state vector and  $\underline{\Phi}(t_2, t_1)$  is the state transition matrix between the time instants  $t_1$  and  $t_2$ .

Let us consider first the time interval  $[0, T_1)$  within which the system is time invariant. The transition matrix relating the state vector between two instants  $t_1$  and  $t_2$  belonging to  $[0, T_1)$  is found as [45]

$$\underline{\Phi}_1(t_2, t_1) = \underline{\mathbf{W}}_1(t_2)\underline{\mathbf{W}}_1^{-1}(t_1), \quad (\text{A2})$$

where  $\underline{\mathbf{W}}_1(t)$  is the Wronskian matrix of the solutions in the time interval  $[0, T_1)$ . Using the general Wronskian matrix properties

$$\underline{\mathbf{W}}^{-1}(t) = \underline{\mathbf{W}}(-t), \quad (\text{A3})$$

$$\underline{\mathbf{W}}(t_2)\underline{\mathbf{W}}(t_1) = \underline{\mathbf{W}}(t_2 + t_1), \quad (\text{A4})$$

the transition matrix between time instants  $t_1$  and  $t_2$  when they belong to the time interval  $T_1$  is

$$\begin{aligned} \underline{\Phi}_1(t_2, t_1) &= \underline{\mathbf{W}}_1(t_2)\underline{\mathbf{W}}_1^{-1}(t_1) = \underline{\mathbf{W}}_1(t_2)\underline{\mathbf{W}}_1(-t_1) \\ &= \underline{\mathbf{W}}_1(t_2 - t_1). \end{aligned} \quad (\text{A5})$$

Analogously, the transition matrix between time instants  $t_1$  and  $t_2$  when they belong to the time interval  $T_2$  is  $\underline{\Phi}_2(t_2, t_1) = \underline{\mathbf{W}}_2(t_2 - t_1)$ .

Accordingly, when  $t_1$  and  $t_2$  are within two adjacent different time intervals, the state transition matrix reads as

$$\underline{\Phi}(t_2, t_1) = \underline{\Phi}_2(t_2, t_c)\underline{\Phi}_1(t_c, t_1) = \underline{\mathbf{W}}_2(t_2 - t_c)\underline{\mathbf{W}}_1(t_c - t_1), \quad (\text{A6})$$

where  $t_c$  is the critical time instant at which the system coefficient changes (i.e., at  $t = t_c = T_1$ ), and the subscripts  $j = 1, 2$  of  $\underline{\mathbf{W}}_j$  denote the two different time intervals of lengths  $T_1$  and  $T_2$ . As an example, we consider the *LC*

resonator with time-variant capacitor, where the two Wronskian matrices of the solutions associated with each time interval,  $T_j$  are given by

$$\underline{\mathbf{W}}_j(t) = \begin{bmatrix} \cos \Omega_j t & \frac{1}{\Omega_j} \sin \Omega_j t \\ -\Omega_j \sin \Omega_j t & \cos \Omega_j t \end{bmatrix}, \quad (\text{A7})$$

where  $\Omega_j = (L_0 C_j)^{-1/2}$  with  $j = 1, 2$  are the resonance frequencies of the *LC* resonator in the time intervals  $T_1$  and  $T_2$ , respectively. Therefore, the state transition matrices at different time instants  $\chi$  for different pieces of the time-variant capacitor read as

$$\underline{\Phi}(\chi, 0) = \underline{\Phi}_1(\chi, 0) = \begin{bmatrix} \cos \Omega_1 \chi & \frac{1}{\Omega_1} \sin \Omega_1 \chi \\ -\Omega_1 \sin \Omega_1 \chi & \cos \Omega_1 \chi \end{bmatrix}, \quad (\text{A8})$$

if  $0 < \chi \leq T_1$ , or

$$\begin{aligned} \underline{\Phi}(\chi, 0) &= \underline{\Phi}_2(\chi, T_1)\underline{\Phi}_1(T_1, 0) \\ &= \begin{bmatrix} \cos \Omega_2(\chi - T_1) & \frac{1}{\Omega_2} \sin \Omega_2(\chi - T_1) \\ -\Omega_2 \sin \Omega_2(\chi - T_1) & \cos \Omega_2(\chi - T_1) \end{bmatrix} \\ &\quad \begin{bmatrix} \cos \Omega_1 T_1 & \frac{1}{\Omega_1} \sin \Omega_1 T_1 \\ -\Omega_1 \sin \Omega_1 T_1 & \cos \Omega_1 T_1 \end{bmatrix}, \end{aligned} \quad (\text{A9})$$

if  $T_1 < \chi \leq T_m$ . Using the state transition matrices in (A8) and (A9), one can find the solution to the evolution equation in (2) knowing the initial state of the system. Note that the derived transition matrix  $\underline{\Phi}(T_m, 0)$  obtained by substituting  $\chi = T_m$  in (A9) is equal to the one given in (4).

- 
- [1] J. Wiersig, Enhancing the Sensitivity of Frequency and Energy Splitting Detection by Using Exceptional Points: Application to Microcavity Sensors for Single-Particle Detection, *Phys. Rev. Lett.* **112**, 203901 (2014).
  - [2] W. Chen, Ş. Kaya Özdemir, G. Zhao, J. Wiersig, and L. Yang, Exceptional points enhance sensing in an optical microcavity, *Nature* **548**, 192 (2017).
  - [3] F. Vollmer and L. Yang, Review label-free detection with high-Q microcavities: A review of biosensing mechanisms for integrated devices, *Nanophotonics* **1**, 267 (2012).
  - [4] L. He, Ş. K. Özdemir, J. Zhu, W. Kim, and L. Yang, Detecting single viruses and nanoparticles using whispering gallery microlasers, *Nat. Nanotechnol.* **6**, 428 (2011).
  - [5] Y. Liu, J. A. R. Williams, and I. Bennion, Optical bend sensor based on measurement of resonance mode splitting of long-period fiber grating, *IEEE Photonics Technol. Lett.* **12**, 531 (2000).
  - [6] W. W. Chow, J. Gea-Banacloche, L. M. Pedrotti, V. E. Sanders, W. Schleich, and M. O. Scully, The ring laser gyro, *Rev. Mod. Phys.* **57**, 61 (1985).



- [7] S. Sunada and T. Harayama, Design of resonant microcavities: Application to optical gyroscopes, *Opt. Express* **15**, 16245 (2007).
- [8] C. E. Rüter, K. G. Makris, R. El-Ganainy, D. N. Christodoulides, M. Segev, and D. Kip, Observation of parity–time symmetry in optics, *Nat. Phys.* **6**, 192 (2010).
- [9] H. Ramezani, T. Kottos, R. El-Ganainy, and D. N. Christodoulides, Unidirectional nonlinear PT-symmetric optical structures, *Phys. Rev. A* **82**, 043803 (2010).
- [10] J. Schindler, A. Li, M. C. Zheng, F. M. Ellis, and T. Kottos, Experimental study of active LRC circuits with PT symmetries, *Phys. Rev. A* **84**, 040101 (2011).
- [11] M. Kulishov and B. Kress, Distributed Bragg reflector structures based on PT-symmetric coupling with lowest possible lasing threshold, *Opt. Express* **21**, 22327 (2013).
- [12] H. Hodaei, M.-A. Miri, M. Heinrich, D. N. Christodoulides, and M. Khajavikhan, Parity-time–symmetric microring lasers, *Science* **346**, 975 (2014).
- [13] M. Y. Nada, M. A. K. Othman, and F. Capolino, Theory of coupled resonator optical waveguides exhibiting high-order exceptional points of degeneracy, *Phys. Rev. B* **96**, 184304 (2017).
- [14] M. A. K. Othman, V. Galdi, and F. Capolino, Exceptional points of degeneracy and PT symmetry in photonic coupled chains of scatterers, *Phys. Rev. B* **95**, 104305 (2017).
- [15] H. Hodaei, A. U. Hassan, S. Wittek, H. Garcia-Gracia, R. El-Ganainy, D. N. Christodoulides, and M. Khajavikhan, Enhanced sensitivity at higher-order exceptional points, *Nature* **548**, 187 (2017).
- [16] M. Veysi, M. A. K. Othman, A. Figotin, and F. Capolino, Degenerate band edge laser, *Phys. Rev. B* **97**, 195107 (2018).
- [17] C. M. Bender and S. Boettcher, Real Spectra in Non-Hermitian Hamiltonians Having PT Symmetry, *Phys. Rev. Lett.* **80**, 5243 (1998).
- [18] A. F. Abdelshafy, M. A. K. Othman, D. Oshmarin, A. Almutawa, and F. Capolino, Exceptional points of degeneracy in periodically-coupled waveguides and the interplay of gain and radiation loss: Theoretical and experimental demonstration, arXiv:180905256.
- [19] A. Guo, G. J. Salamo, D. Duchesne, R. Morandotti, M. Volatier-Ravat, V. Aimez, G. A. Siviloglou, and D. N. Christodoulides, Observation of PT-Symmetry Breaking in Complex Optical Potentials, *Phys. Rev. Lett.* **103**, 093902 (2009).
- [20] T. Stehmann, W. D. Heiss, and F. G. Scholtz, Observation of exceptional points in electronic circuits, *J. Phys. Math. Gen.* **37**, 7813 (2004).
- [21] A. Figotin and I. Vitebskiy, Nonreciprocal magnetic photonic crystals, *Phys. Rev. E* **63**, 066609 (2001).
- [22] A. Figotin and I. Vitebskiy, Oblique frozen modes in periodic layered media, *Phys. Rev. E* **68**, 036609 (2003).
- [23] A. Figotin and I. Vitebskiy, Gigantic transmission band-edge resonance in periodic stacks of anisotropic layers, *Phys. Rev. E* **72**, 036619 (2005).
- [24] A. Figotin and I. Vitebskiy, Slow-wave resonance in periodic stacks of anisotropic layers, *Phys. Rev. A* **76**, 053839 (2007).
- [25] N. Apaydin, L. Zhang, K. Sertel, and J. L. Volakis, Experimental validation of frozen modes guided on printed coupled transmission lines, *IEEE Trans. Microw. Theory Tech.* **60**, 1513 (2012).
- [26] N. Gutman, C. Martijn de Sterke, A. A. Sukhorukov, and L. C. Botten, Slow and frozen light in optical waveguides with multiple gratings: Degenerate band edges and stationary inflection points, *Phys. Rev. A* **85**, 033804 (2012).
- [27] J. R. Burr, N. Gutman, C. M. de Sterke, I. Vitebskiy, and R. M. Reano, Degenerate band edge resonances in coupled periodic silicon optical waveguides, *Opt. Express* **21**, 8736 (2013).
- [28] M. A. K. Othman, F. Yazdi, A. Figotin, and F. Capolino, Giant gain enhancement in photonic crystals with a degenerate band edge, *Phys. Rev. B* **93**, 024301 (2016).
- [29] A. M. Zuboraj, B. K. Sertel, and C. J. L. Volakis, Propagation of Degenerate Band-Edge Modes using Dual Non-identical Coupled Transmission Lines, *Phys. Rev. Appl.* **7**, 064030 (2017).
- [30] J. T. Sloan, M. A. K. Othman, and F. Capolino, Theory of double ladder lumped circuits with degenerate band edge, *IEEE Trans. Circuits Syst. Regul. Pap.* **65**, 3 (2018).
- [31] C. D. Meyer, *Matrix Analysis and Applied Linear Algebra* (SIAM: Society for Industrial and Applied Mathematics, Philadelphia, 2001).
- [32] L. Hogben, *Handbook of Linear Algebra* (Chapman and Hall/CRC, 2017), 2nd ed.
- [33] S. L. McCall, A. F. J. Levi, R. E. Slusher, S. J. Pearton, and R. A. Logan, Whispering-gallery mode microdisk lasers, *Appl. Phys. Lett.* **60**, 289 (1992).
- [34] M. A. K. Othman, M. Veysi, A. Figotin, and F. Capolino, Low starting electron beam current in degenerate band edge oscillators, *IEEE Trans. Plasma Sci.* **44**, 918 (2016).
- [35] D. Oshmarin, F. Yazdi, M. A. K. Othman, J. Sloan, M. Radfar, M. M. Green, and F. Capolino, Oscillator based on lumped double ladder circuit with band edge degeneracy, arXiv:161000415.
- [36] M. A. K. Othman, M. Veysi, A. Figotin, and F. Capolino, Giant amplification in degenerate band edge slow-wave structures interacting with an electron beam, *Phys. Plasmas* **23**, 033112 (2016).
- [37] M. A. K. Othman, V. A. Tamma, and F. Capolino, Theory and new amplification regime in periodic multimodal slow wave structures with degeneracy interacting with an electron beam, *IEEE Trans. Plasma Sci.* **44**, 594 (2016).
- [38] M. A. K. Othman and F. Capolino, in 2017 IEEE Int. Symp. Antennas Propag. Usn. Natl. Radio Sci. Meet. (2017), pp. 57–58.
- [39] C. Peng, Z. Li, and A. Xu, Rotation sensing based on a slow-light resonating structure with high group dispersion, *Appl. Opt.* **46**, 4125 (2007).
- [40] N. Moiseyev, Crossing rule for a PT-symmetric two-level time-periodic system, *Phys. Rev. A* **83**, 052125 (2011).
- [41] G. Della Valle and S. Longhi, Spectral and transport properties of time-periodic PT-symmetric tight-binding lattices, *Phys. Rev. A* **87**, 022119 (2013).
- [42] D. Psiachos, N. Lazarides, and G. P. Tsironis, PT-symmetric dimers with time-periodic gain/loss function, *Appl. Phys. A* **117**, 663 (2014).

- [43] F. Battelli, J. Diblík, M. Fečkan, J. Pickton, M. Pospíšil, and H. Susanto, Dynamics of generalized PT-symmetric dimers with time-periodic gain–loss, *Nonlinear Dyn.* **81**, 353 (2015).
- [44] M. Chitsazi, H. Li, F. M. Ellis, and T. Kottos, Experimental Realization of Floquet PT-Symmetric Systems, *Phys. Rev. Lett.* **119**, 093901 (2017).
- [45] John A. Richards, *Analysis of Periodically Time-Varying Systems* (Springer, New York, 1983).
- [46] K. M. Hoffman and R. Kunze, *Linear Algebra* (Pearson, Englewood Cliffs, NJ, 1971), 2nd ed.
- [47] G. H. Heilmeyer, An analysis of parametric amplification in periodically loaded transmission lines, *RCA Rev.* **20**, 442 (1959).
- [48] P. Penfield and R. P. Rafuse, *Varactor Applications* (MIT Press, Cambridge, 1962).
- [49] R. E. Collin, *Foundations for Microwave Engineering* (Wiley-IEEE Press, New York, 2001), 2nd ed.
- [50] E. Vincent, R. Gribonval, and C. Fevotte, Performance measurement in blind audio source separation, *IEEE Trans. Audio Speech Lang. Process.* **14**, 1462 (2006).
- [51] C. A. Desoer and M. Y. Wu, Stability of multiple-loop feedback linear time-invariant systems, *J. Math. Anal. Appl.* **23**, 121 (1968).
- [52] A. Welters, On explicit recursive formulas in the spectral perturbation analysis of a Jordan block, *SIAM J. Matrix Anal. Appl.* **32**, 1 (2011).